Demonstration of nondegenerate spectrum reversal in optical-frequency regime

Chenji Gu,* Boaz Ilan, and Jay E. Sharping

School of Natural Sciences, University of California, Merced, California 95343, USA

**Corresponding author: cgu2@ucmerced.edu*

Received November 30, 2012; revised January 20, 2013; accepted January 24, 2013; posted January 25, 2013 (Doc. ID 180959); published February 14, 2013

This Letter reports theoretical and experimental studies of spectrum reversal with tunable wavelength offset in the optical-frequency regime—two widely separated spectral sidebands can always behave as mirror images of one another with respect to the center frequency of the controlling pump pulse. We call this interesting physical phenomenon "spectral mirror imaging." © 2013 Optical Society of America

OCIS codes: 060.2320, 060.4370, 060.5295.

The concept of temporal phase conjugation (TPC), also known as midspan spectral inversion, can be traced back two decades when TPC was used to compensate for pulse broadening due to chromatic dispersion in optical fibers [1,2]. Careful characterizations of the optical fields, in particular the shapes of the spectral envelopes [3,4], were not undertaken due to the need for broadband ultrashort light sources and sophisticated diagnostic techniques [5,6]. In this Letter we report, to the best of our knowledge, the first experimental observations of tunable nondegenerate spectrum reversal arising from partially degenerate four-wave mixing (FWM) in optical fibers. Our simulations along with experimental measurements show that two spectral sidebands are mirror images of one another with respect to the center frequency of the input pump field. We call this phenomenon "spectral mirror imaging" (SMI). These features are revealed in both the femtosecond and picosecond domains.

Our exploration of SMI, while fundamentally interesting, also has enormous potential for applicability. Recently, advanced *temporal imaging systems* have been demonstrated based on forward partially degenerate FWM processes. These systems perform all-optical ultrafast waveform characterization tasks such as time-to-frequency conversion [7], temporal waveform magnification [8], and packet compression [9]. The key component is the time lens, which imparts a quadratic phase modulation onto the input signal pulse through the nonlinear wave-mixing with a chirped (i.e., a quadratic variation of the temporal phase) pump pulse. Here by using unchirped pump pulses, rather than the configuration for time lenses, we demonstrate *spectral imaging systems*. Interestingly, SMI-based *spectral mirrors*, when combined with *time lenses*, will complete a set of novel optical components for manipulating temporal and spectral information in ways analogous to traditional imaging.

The relationship between SMI and TPC is illustrated in Fig. 1(a). The electric fields of two copropagating optical pulses ($k = 1, 2$), after passing through a designed SMI system, are given by $E_k(t) = A_k(t) \cdot e^{-i\omega_k t}$, where $A_k(t)$ are the slowly varying complex envelopes independent of the rapidly varying carrier waves $e^{-i\omega_k t}$. In the frequency domain, the spectra of these two pulses are given by the Fourier transform $\mathcal{F}\{A_k(t)\} = \tilde{A}_k(\omega) = \tilde{E}_k(\omega + \omega_k)$, where $\tilde{A}_k(\omega)$ represent the spectra of each pulse centered on its own reference frame. On one hand, SMI implies that the spectral amplitudes are reversed relative to each other, i.e., $|\tilde{A}_2(\omega)| = |\tilde{A}_1(-\omega)|$. Since the carrier frequencies of the two waves can be different, these two spectra are distributed as mirror images of one another with respect to the mean of two carrier frequencies, i.e., $(\omega_1 + \omega_2)/2$. We refer to the long-wavelength sideband as the *signal* and the short-wavelength sideband as the *idler*. Due to energy conservation through the optical parametric process, the center frequencies of the two sidebands and the center frequency of the pump are related as $\omega_1 + \omega_2 = 2\omega_0$. Therefore, as shown in the bottom of Fig. 1(a), in absolute frequency space two spectral sidebands are equally separated with respect to the center frequency of pump.

On the other hand, TPC implies that the temporal phase profiles of two pulses are inverted, i.e., $\arg\{A_2(t)\} =$

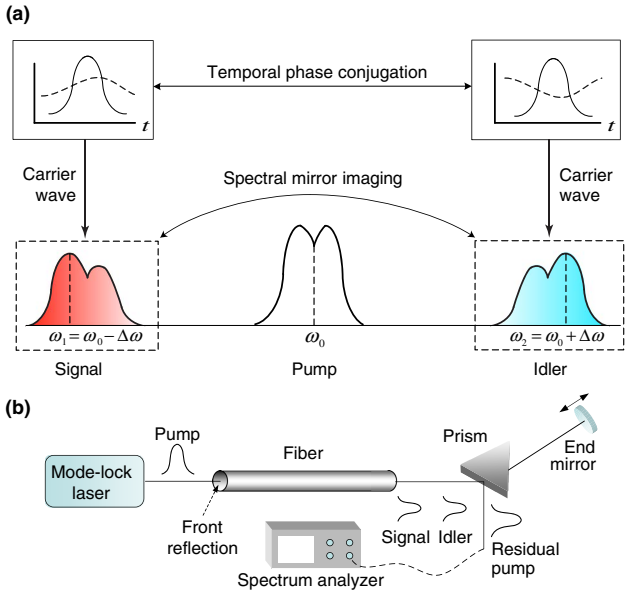

Fig. 1. (Color online) (a) Concept of SMI. Two pulses, signal and idler, are depicted at the top left and right, respectively, where the solid curves are the temporal amplitudes $|A_{1,2}(t)|$ and the dashed curves are the temporal phase profiles $\arg\{A_{1,2}(t)\}$. Their spectral amplitudes $|\tilde{A}_{1,2}(\omega)|$ are depicted at the bottom left and right with different center frequencies $\omega_{1,2}$. (b) Schematic of an SMI system.

$\varphi_0 - \arg\{A_1(t)\}$, where φ_0 is a constant representing arbitrary absolute phase. Furthermore, if the amplitudes of two pulses are the same, their complex envelopes are related as $A_2(t) = A_1^*(t) \cdot e^{i\varphi_0}$. The relationship between SMI and TPC follows from the Fourier transform:

$$\tilde{A}_2(\omega) = \mathcal{F}[A_2(t)] = \mathcal{F}[A_1^*(t) \cdot e^{i\varphi_0}] = \tilde{A}_1^*(-\omega)e^{i\varphi_0}. \quad (1)$$

Therefore SMI is a spectral realization of TPC. The overall concept is similar to low sideband modulation in communications and signal processing, where the generated spectrum is inverted with respect to the baseband spectrum. This concept also resembles radio-frequency conversion mixing, where an inverted spectrum is achieved by using high-side local oscillation injection [10].

Our demonstration of SMI involves a partially degenerate FWM process, modeled as the interaction among three waves (i.e., pump, signal, and idler) using three coupled nonlinear Schrödinger equations [11]:

$$\frac{\partial A_0}{\partial z} - i\gamma[|A_0|^2 + 2|A_1|^2 + 2|A_2|^2]A_0 + 2i\gamma A_1 A_2 A_0^* e^{i\Delta\beta z} = 0, \quad (2)$$

$$\frac{\partial A_1}{\partial z} + \Delta\beta_{11}\frac{\partial A_1}{\partial T} + \frac{i}{2}\beta_{21}\frac{\partial^2 A_1}{\partial T^2} - i\gamma[|A_1|^2 + 2|A_2|^2 + 2|A_0|^2]A_1 + i\gamma A_0^2 A_2^* e^{-i\Delta\beta z} = 0, \quad (3)$$

$$\frac{\partial A_2}{\partial z} + \Delta\beta_{12}\frac{\partial A_2}{\partial T} + \frac{i}{2}\beta_{22}\frac{\partial^2 A_2}{\partial T^2} - i\gamma[|A_2|^2 + 2|A_1|^2 + 2|A_0|^2]A_2 + i\gamma A_0^2 A_1^* e^{-i\Delta\beta z} = 0. \quad (4)$$

Equations (2)–(4) consider the copropagation of three waves in the moving frame of the pump pulse, where A_0, A_1, and A_2 represent pump, signal, and idler, respectively. The pump wavelength is near the zero dispersion wavelength (ZDW) of fiber ($\beta_{20} = 0$), the nonlinearity of fiber is γ, and the fiber loss is negligible. The group-velocity difference (GVD) between the pump and signal pulses is defined as $\Delta\beta_{11} = \beta_1(\omega_1) - \beta_1(\omega_0)$, and the difference between the pump and idler is defined as $\Delta\beta_{12} = \beta_1(\omega_2) - \beta_1(\omega_0)$. The GVDs of the signal and idler are described by β_{21} and β_{22}, while the propagation mismatch is described by $\Delta\beta = \beta(\omega_1) + \beta(\omega_2) - 2\beta(\omega_0)$.

Our experimental setup for the demonstration of SMI illustrated in Fig. 1(b) is based on fiber optical parametric oscillators (FOPOs) [12–14], which can be modeled as a single-pass fiber optical parametric process upon steady-state operation [13]. A Fabry–Perot cavity is formed between the Fresnel reflection from the front cleave of the photonic-crystal fiber and the end mirror. We use two FOPOs, one pumped by a femtosecond laser and the other pumped by a picosecond laser. The femtosecond FOPO is pumped by a mode-locked Yb-doped fiber laser that delivers a pulse duration of 400 fs with a repetition rate of 50 MHz. It is linearly polarized with center wavelength at 1032 nm. The average pump power launched into the fiber is 620 mW. In the femtosecond case, the fiber is 3 cm long with a ZDW at 1030 nm [14]. The picosecond FOPO is pumped by a mode-locked Nd:vanadate laser that delivers transform-limited 8 ps pulses at a repetition rate of 80 MHz. It is linearly polarized with center wavelength at 1064 nm. The average pump power coupled into the fiber is 525 mW. In the picosecond case, the fiber is 1.2 m long with ZDW at 1061 nm [13].

The spectra plotted in Fig. 2(a) are the output of the femtosecond system where traces 1, 2, and 3 correspond to three different end mirror translation settings. In each trace, from left to right, the broadband spectrum includes a signal sideband, a residual pump, and an idler sideband. Trace 1 is obtained when the FOPO is operated at its highest output power. We acquire traces 2 and 3 by reducing 15 and 30 μm of cavity length (corresponding to 0.1 and 0.2 ps round-trip delay) of the FOPO, respectively. In these three traces we observe two distinct sidebands located at about 7880 and 11500 cm^{-1}, which are equally spaced from the pump at 9690 cm^{-1}. In trace 1 each sideband includes three peaks. As the cavity length becomes shorter, in trace 2 each sideband has two peaks. Finally, in trace 3 there is only one peak on each sideband. In all cases, the signal and the idler behave as mirror images of one another. Simulations for the femtosecond case, shown in Figs. 2(b) and 2(c), support our experimental observations.

Figure 3(a) shows the experimental observations of SMI for the picosecond system. Two distinct sidebands

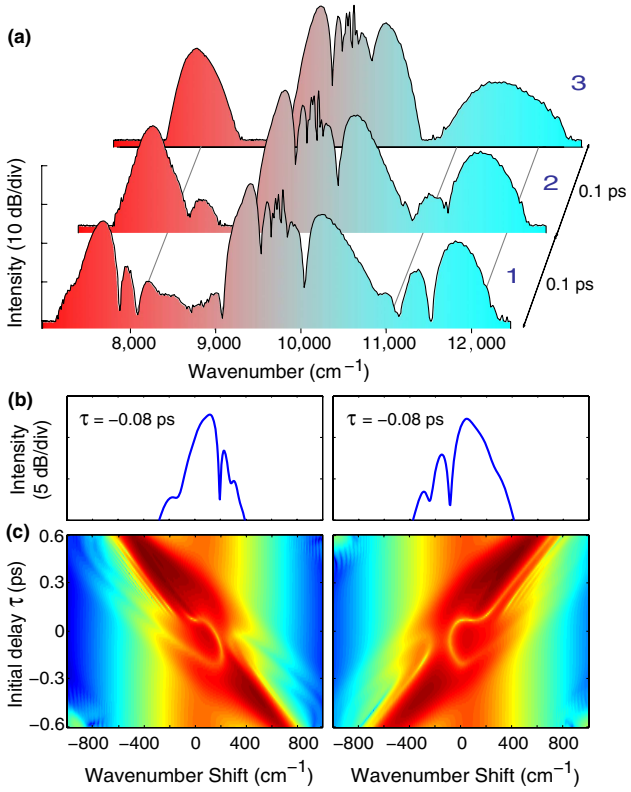

Fig. 2. (Color online) Demonstration of SMI in the femtosecond domain. (a) Measured output spectrum from the femtosecond FOPO. (b) Simulations of two spectral sidebands in the presence of a femtosecond pump pulse. The resulting spectra at $\tau = -80$ fs resemble the experimental measurement in trace 1. (c) Simulations of two sideband spectrograms.

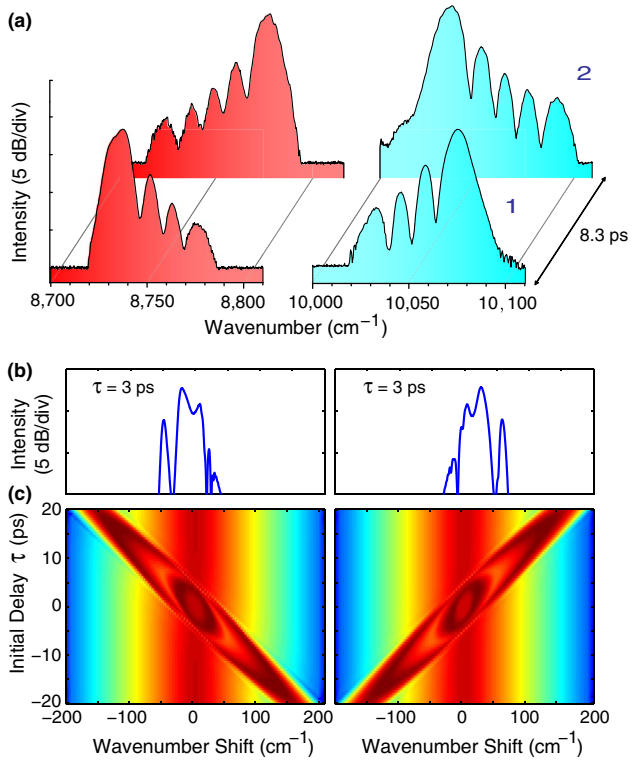

Fig. 3. (Color online) Demonstration of SMI in the picosecond domain. (a) Measured output spectrum from the picosecond FOPO. (b) Simulations of two spectral sidebands in the presence of a picosecond pump pulse. The resulting spectra at $\tau = 3$ ps resemble the experimental measurement in trace 1. (c) Simulations of two sideband spectrograms.

(left for signal and right for idler), located at about 8750 and 10050 cm^{-1}, are equally separated from the pump at 9400 cm^{-1}. In trace 1 of Fig. 3(a), the signal exhibits a blue shift with four decaying peaks, while the idler features the mirror image—a red shift with four decaying peaks. Trace 2 in Fig. 3(a) is obtained by increasing the cavity length by 1.25 mm (8.3 ps round-trip delay). In this case the signal exhibits a red shift with five peaks, while the idler exhibits the mirror image—a blue shift with five peaks. Simulations for the picosecond case are shown in Figs. 3(b) and 3(c).

Our simulations are based on Eqs. (2)–(4), with a transform-limited pump pulse and a chirped signal pulse as inputs at $z = 0$. The signal is ahead of the pump when $\tau < 0$. Adding chirp to the input signal pulse is necessary due to the prism inside the cavity, as shown in Fig. 1(b). Assuming opposite chirped idler and signal pulses at the input, which are synchronized, the pump, signal, and idler inputs are as follows:

$$A_0(0,T) = \sqrt{P_0}e^{-\frac{(T+\tau)^2}{2T_0^2}},$$
$$A_1(0,T) = \sqrt{P_1}\,\mathrm{sech}\left(\frac{T}{T_1}\right)e^{-\frac{iCT^2}{T_1^2}} = A_2^*(0,T), \quad (5)$$

where P_0 and P_1 are peak powers, T_0 and T_1 are pulse durations, and C is chirp. In the femtosecond case, we use $T_0 = 400$ fs, $P_0 = 30$ kW, $T_1 = 80$ fs, $P_1 = 10$ W, and $C = -5$. In the picosecond case, we use $T_0 = 8$ ps, $P_0 = 780$ W, $T_1 = 2$ ps, $P_1 = 5$ W, and $C = -10$.

In summary, we explore SMI features in both femtosecond and picosecond domains. As a spectral realization of phase conjugation, SMI offers a measurable connection between the temporal and spectral properties of correlated optical fields.

We thank Prof. Kenneth K. Y. Wong and Prof. Kevin A. Mitchell for their comments. This work was supported by AFOSR Young Investigator.

References

1. S. Watanabe, T. Naito, and T. Chikama, IEEE Photon. Technol. Lett. **5**, 92 (1993).
2. A. H. Gnauck, R. M. Jopson, and R. M. Derosier, IEEE Photon. Technol. Lett. **5**, 663 (1993).
3. K. Mori, T. Morioka, and M. Saruwatari, Opt. Lett. **21**, 110 (1996).
4. K. Inoue, Opt. Lett. **22**, 1772 (1997).
5. R. Trebino, *Frequency-Resolved Optical Gating: the Measurement of Ultrashort Laser Pulses* (Kluwer, 2002).
6. C. Iaconis and I. A. Walmsley, Opt. Lett. **23**, 792 (1998).
7. M. A. Foster, R. Salem, D. F. Geraghty, A. C. Turner-Foster, M. Lipson, and A. L. Gaeta, Nature **456**, 81 (2008).
8. R. Salem, M. A. Foster, A. C. Turner, D. F. Geraghty, M. Lipson, and A. L. Gaeta, Opt. Lett. **33**, 1047 (2008).
9. M. A. Foster, R. Salem, Y. Okawachi, A. C. Turner-Foster, M. Lipson, and A. L. Gaeta, Nat. Photonics **3**, 581 (2009).
10. P. Vizmuller, *RF Design Guide Systems, Circuits and Equations* (Artech House, 1995).
11. S. Wabnitz and J. M. Soto-Crespo, Opt. Lett. **23**, 265 (1998).
12. J. E. Sharping, J. Lightwave Technol. **26**, 2184 (2008).
13. C. Gu, C. Goulart, and J. E. Sharping, Opt. Lett. **36**, 1488 (2011).
14. C. Gu, H. Wei, S. Chen, W. Tong, and J. E. Sharping, Opt. Lett. **35**, 351 (2010).